Table of contents

S1 Overview of measurements

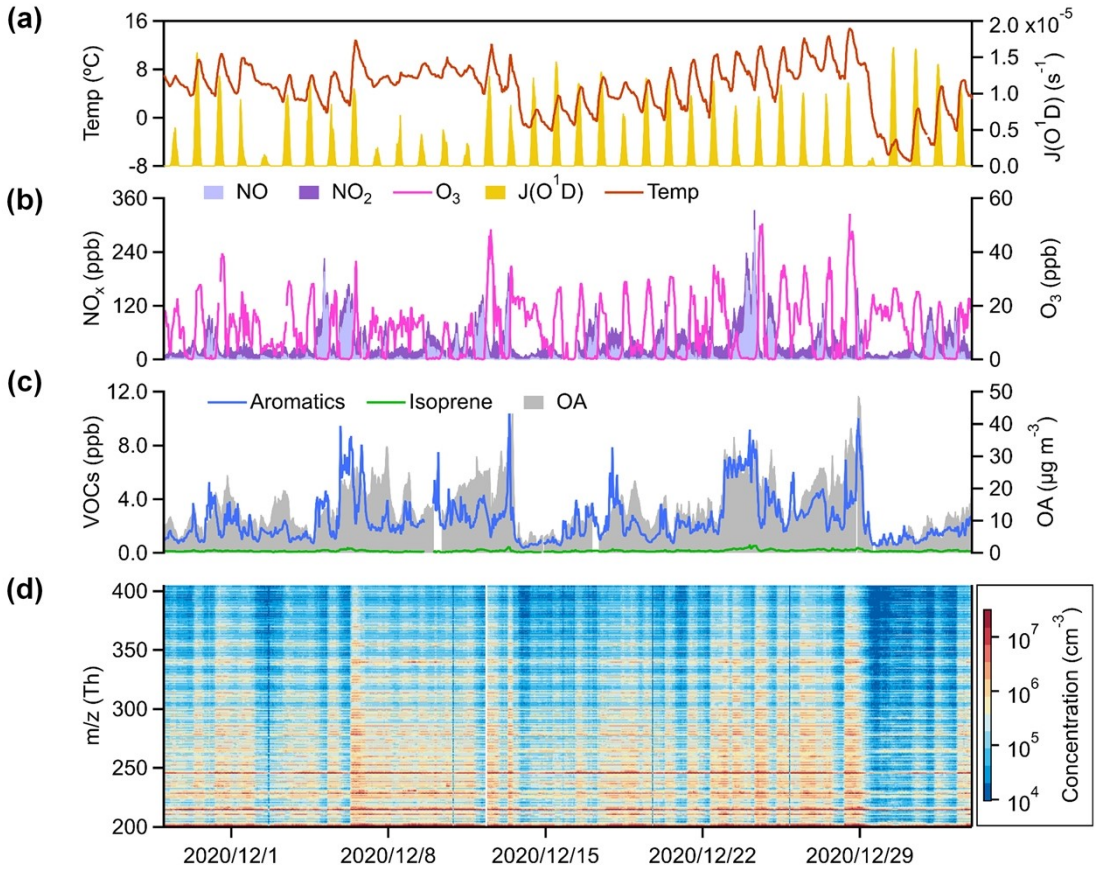

Fig. S1 Overview of measurements during the campaign. Time series of (a) temperature (Temp) and the photolysis frequency of O_3 (JO^1D); (b) O_3 and NO_x ($NO + NO_2$); (c) total aromatics (benzene + toluene + C_8 aromatics + C_9 aromatics + C10 aromatics + styrene), isoprene, and OAs; and (d) mass spectra of the nitrate CI-APi-TOF with m/z

in the range of 203–404 Th.

S2 binPMF analysis

S2.1 binPMF inputs

Data matrix

As described in Zhang et al.[1], we divided the mass spectra measured by nitrate CI-APi-TOF into small bins of 0.006 Th width and performed the baseline subtraction and mass axis calibration. Figure S2 shows the averaged binned spectrum with marked deleted bins that nitrated phenol and some fluorinated contaminations (Table S1) that are not our main focus. Besides, we selected the mass bins in the range of 203-404 Th with an appropriate signal-to-noise ratio (SNR > 0.9) as data matrix for binPMF input, neglecting quite weak signals to reduce unnecessary computation.

Table S1. Peak list of deleted bins

Mass-to-charge (Th)	Formulas
201.0153	$C_6H_5NO_3(NO_3^-)$
215.0310	$C_7H_7NO_3(NO_3^-)$
223.8617	$ICl(NO_3^-)$
229.0466	$C_8H_9\ NO_3\ (NO_3^-)$
246.0004	$C_6H_4N_2O_5c$
250.8807	$IONO_2(NO_3^-)$
264.0110	$C_6H_5NO_3(HNO_3NO_3^-)$

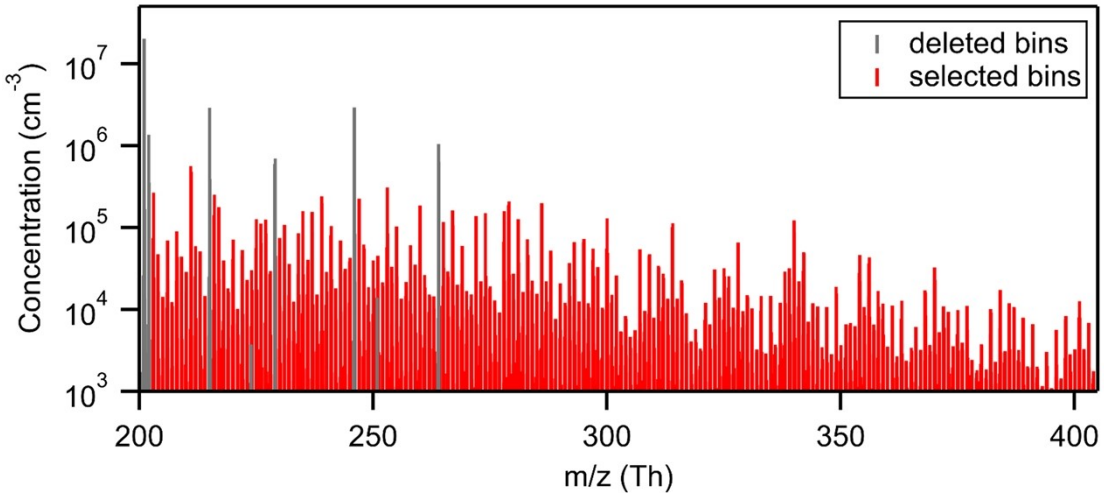

Fig. S2 The averaged binned spectrum. The delete bins (gray) listed in Table S1, other bins (red) with unit m/z in the range of 203-404 Th were adopted as data matrix for PMF inputs.

Error matrix

The error matrix was calculated by Eq. (1)[2]

$$S_{ij} = \sigma_{ij} + \sigma_{noise} \quad (1)$$

where S_{ij} is estimated the measurement uncertainty of m/z j at time i, σ_{ij} represents the analytical uncertainty from counting statistics and σ_{noise} is the standard deviation of instrument noise. σ_{ij} is estimated as follows:

$$\sigma_{ij} = a \times \frac{\sqrt{I_{ij}}}{\sqrt{t}} \quad (2)$$

where I is the signal intensity term, in unit of ions per second; t stands for length of averaging in seconds, and a is an empirical coefficient to compensate for unaccounted uncertainties[3, 4] and is 1.28 in this study as previously estimated from laboratory experiments[4]. The σ term was estimated as the median of the standard deviations from signals in the bins in the region between nominal masses, where no physically meaningful signals are expected.

S2.2 Diagnostics

It is the most critical to select a proper number of factors towards interpreting the PMF results. The Q/Q_{exp} value is one of the main mathematical diagnoses to PMF results[4-6]. For our PMF result, when the number of factor solution exceeds 8, the rate of decline in Q/Q_{exp} value slowed down (Fig. S3(a)). The unexplained fraction decreased from 20% to 10% from 1- to 8-factor solution and then decreased slowly in subsequent solutions (Fig. S3(b)). Based on the mathematical diagnostics, we should select an appropriate solution from 9-20 factors. The evolution of PMF solutions should been noticed carefully, since solutions with more factors can interpret subtler processes, but too many factors will split a significant factor into unrealistic ones. The main factors with first occurrences are marked in the corresponding solutions (Fig. S3 (a)). As we can see, the O_3-related-I factor is separated first in the 3-factor solution, while the O_3-related-II factor first appear purely in the 12-factor solution and the MT-mixed-OOM factor is separated first in the 13-factor solution. For more than 14-factor solutions, this is more difficult to interpret because they do not provide new physically meaningful factor and will make the main factor split and uncorrelated with external tracers.

We used the rotational ambiguity with setting the fpeak to increase from -1.0 to 1.0 with a difference of 0.2 to check the 13-factor solution (Fig. S3(c)). All solutions are divided into two type solutions, one containing 12 + 'MT-mixed-OOM' factors and the other containing 12 + 'NP-mixed' factors. The 'MT-mixed-OOM' factor contains potential monoterpene-derived OOMs mixing other anthropogenic OOMs. The 'NP-mixed' factor consists of mainly by nitrated phenol which are not our main concern. Finally, the solution with a fpeak value of -0.2 is selected to analysis data. It is currently difficult to prove that the PMF solution we chose is optimal, but it is certain that this solution separates enough information for understanding OOMs.

Meanwhile, it is should be point out that when naming these factors, we prioritize the description of dominated species or their precursors, but if the precursors are complex

mixtures, our naming highlights the characteristics of the chemical processes that drive certain factors.

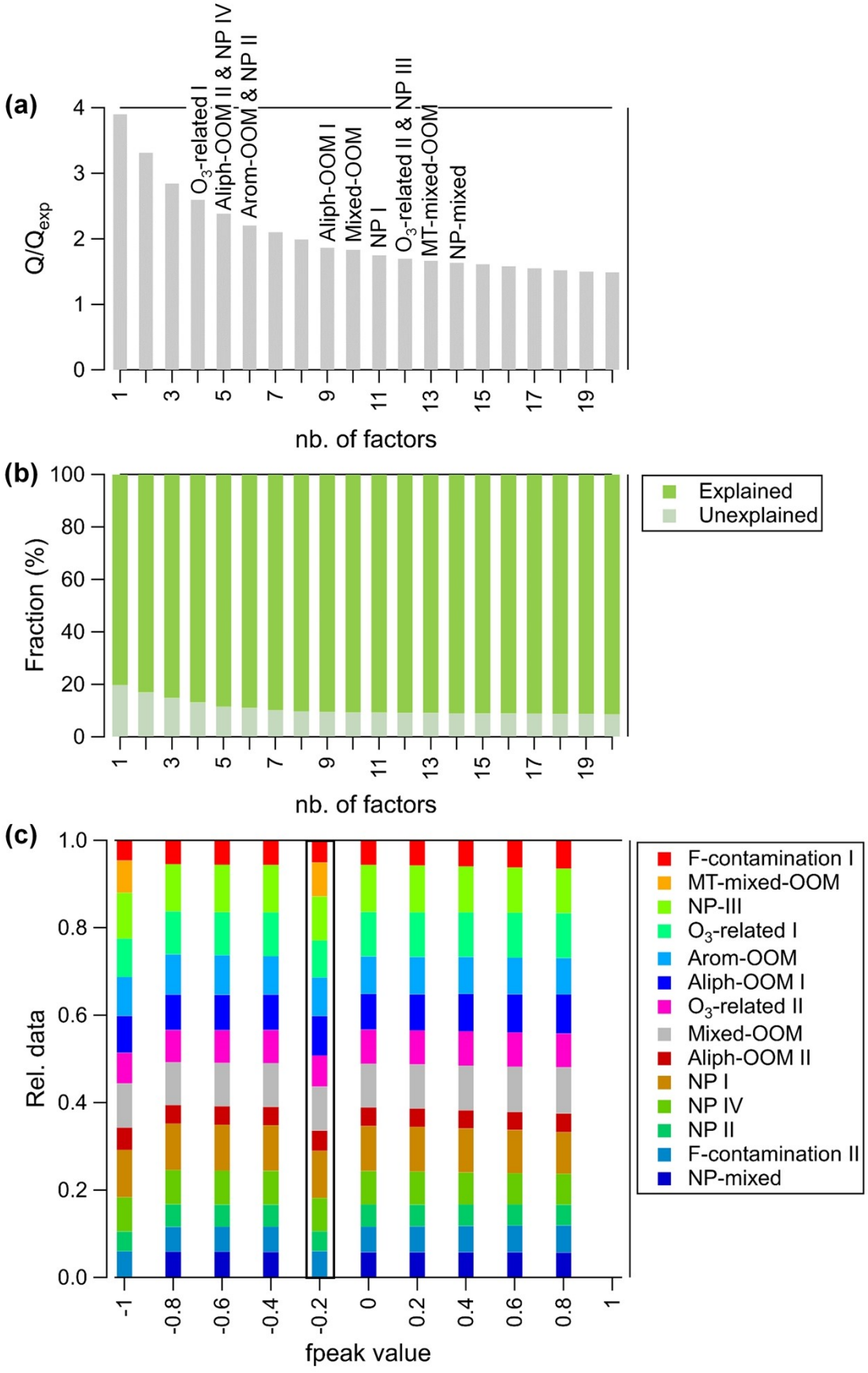

Fig. S3 The diagnostics of PMF solution. (a)Q/Q_{exp}, (b) the explained and unexplained fraction in PMF results, (c) the relative contribution ratio of factors in each solution with different values ([-1,1]) of fpeak.

The residual histograms are a simple and fast method for checking whether the PMF result contains several systematic under- or overestimation. As showed in Fig. S4, the variables of residual appear some compounds with high signal, but we found the most of them are the nitrated phenols like $C_6H_3ClNO_5^-$ (m/z = 203.9705 Th), $C_6H_5NO_4$ (NO_3^-) (m/z = 217.102 Th), $C_7H_7NO_4$ (NO_3^-) (m/z =231.0259Th) and $C_6H_4ClNO_3$(NO_3^-) (m/z =234.9763Th), etc. It is over-split for other physically significant factors if we separate out these compounds. Therefore, it is appropriate to choose the 14-factor solution since the factors about nitrated phenols are not our main concern.

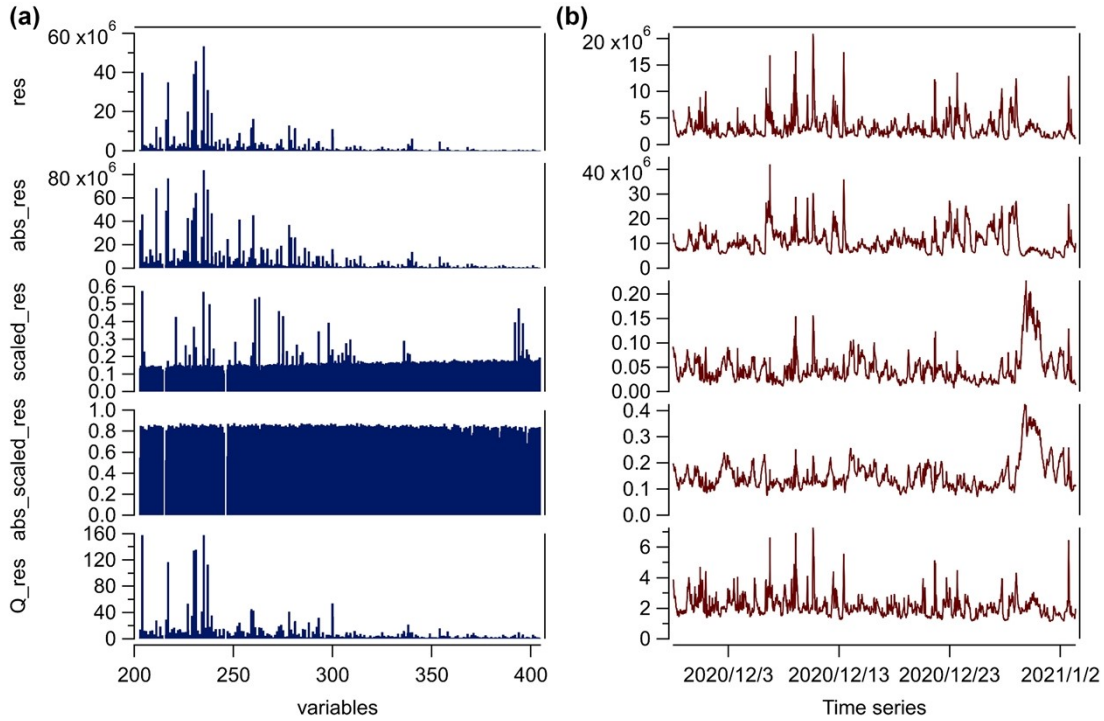

Fig. S4 (a) Mass spectra and (b) time series plots showing the residual histograms of the 13-factor solution.

S2.3 The binPMF result

In summary, we selected 13-factor solution to analysis our dataset.

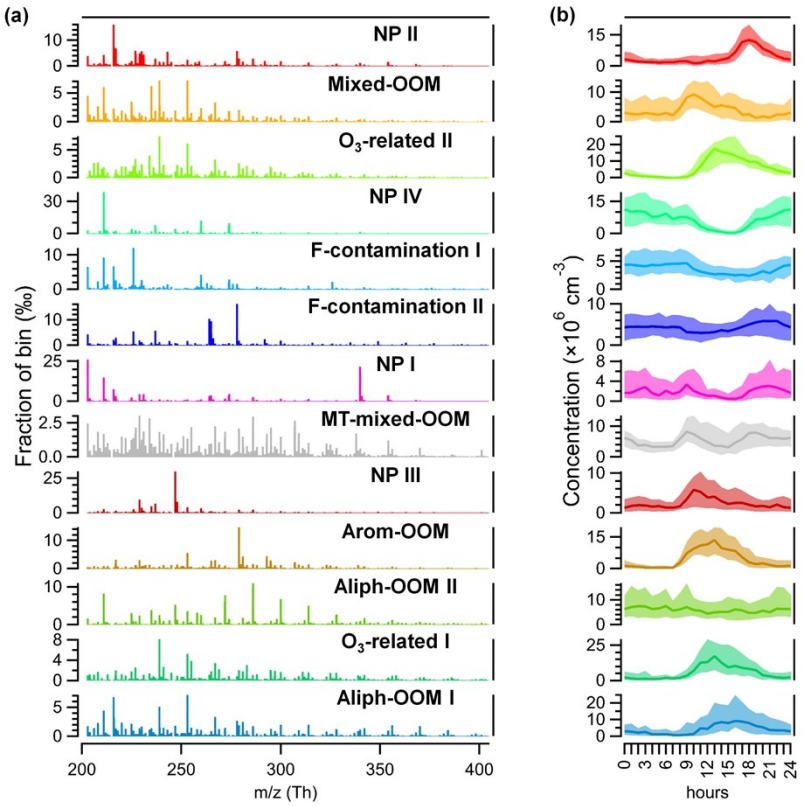

Fig. S5. The binPMF analysis with 13-factor solution. (a) the mass profile, (b) the diurnal pattern.

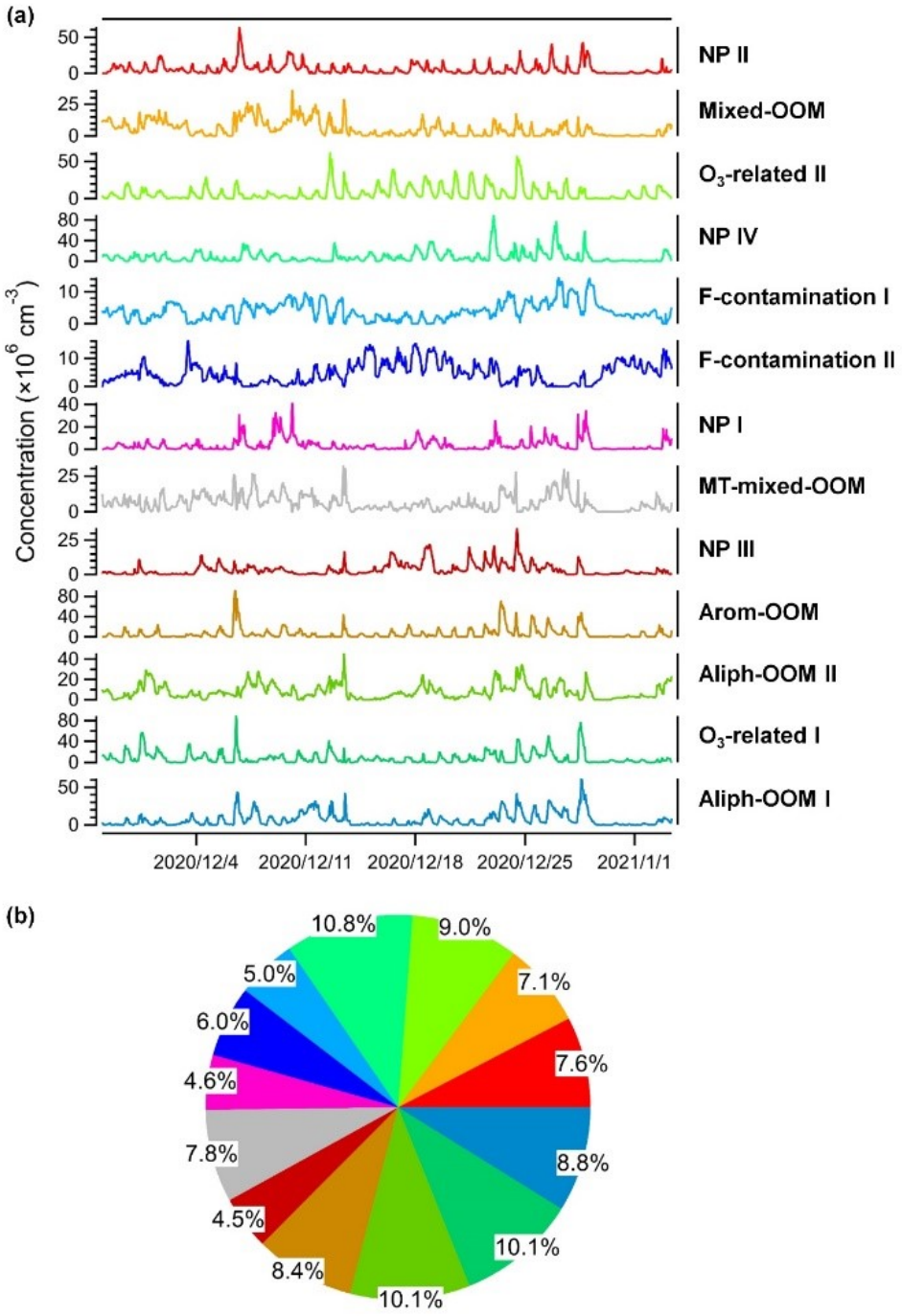

Fig. S6 The binPMF result. (a) the time series, (b) the contribution of each factor to the total signal.

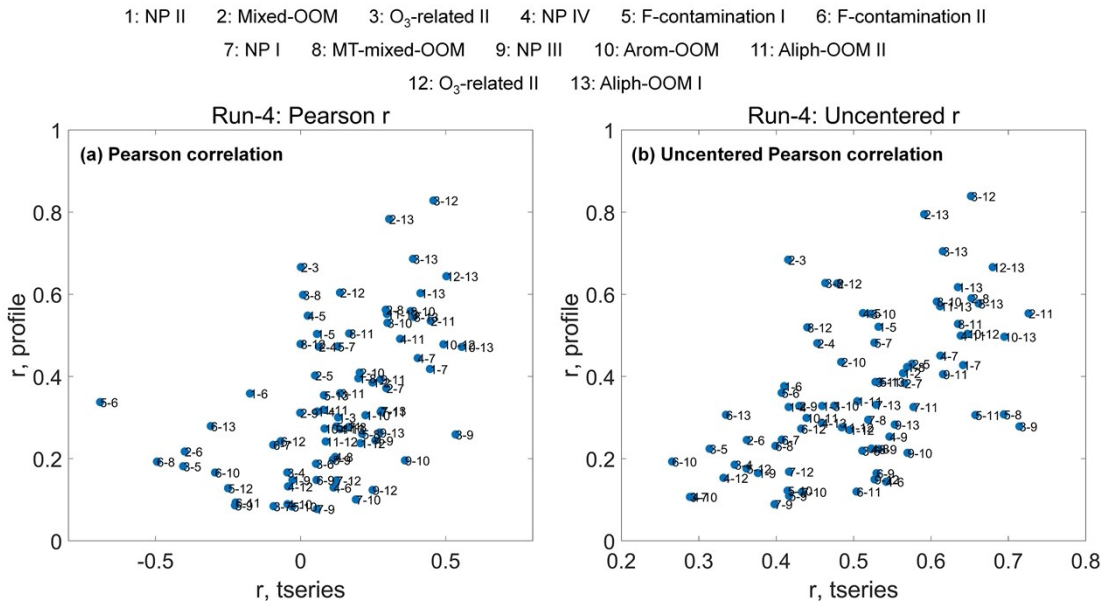

Fig. S7 Comparison among the factors through (a) Pearson correlation and (b) Uncentered Pearson correlation. The x-axis shows the correlation of the time series between the factors, and the y-axis shows the correlation of the spectra between the factors.

S3 Calculation of molecular properties of OOMs

Carbon oxidation state (OS_c)

The OS_c of each **non-nitro** OOM was calculated based on Eq. (3) modified from that in Kroll et al.[7] include organic nitrate contributions:

$$OS_{c=2}(n_O - 3n_N)/n_C - n_H/n_C + n_N/n_C \quad (3)$$

Where n_C, n_H, n_O, and n_N denote the number of carbons, hydrogen, oxygen, and nitrogen in the molecule, respectively.

Double bond equivalent (DBE)

The DBE of each OOM was calculated using Eq. (4), by assuming that all nitrogen come from the nitrate group ($-ONO_2$) or nitro group ($-NO_2$). Here DBE represents the combined effect of double or triple bonds, as well as the ring structure, in the molecule.

$$DBE = n_C + 1 - (n_H + n_N)_{/2} \quad (4)$$

Volatility Basis Set (VBS)

The saturation concentration (volatility) of selected OOMs was estimated based on the group-contribution method proposed by Donahue et al.[8]:

$$log_{10}C^*(300K) = (25 - n_C) \times b_C - (n_O - 2n_N) \times b_O - 2\left[\frac{(n_O - 2n_N) \times n_C}{n_C + n_O - 2n_N}\right] \times b_{CO} \quad (5)$$

Where $b_C = 0.475$, $b_O = 2.3$, $b_{CO} = -0.3$. The effect of nitrate group ($-ONO_2$) on volatility is similar to hydroxyl group (-OH).

The temperature dependence of volatilities is described by Eq. (6), according to Stolzenburg et al.[9]:

$$log_{10}C_i^*(T) = log_{10}C_i^*(300K) + \frac{\Delta H_{vap}}{R \times ln(10)}\left(\frac{1}{300} - \frac{1}{T}\right) \quad (6)$$

The evaporation enthalpy (ΔH_{vap}) can be linked to the saturation mass concentration at 300 K, $\log_{10} C^*(300K)$, according to Donahue et al.[8] and combined with Epstein at al.[10]:

$$\Delta H_{vap}[kJ\ mol^{-1}] = 129 - 5.7 \cdot log_{10}(C^*(300K)) \quad (7)$$

Effective Oxygen Number ($n_{O_{eff}}$)

The effective oxygen number which represents effective oxidation was calculated by Eq. (8), by assuming that all nitrogen of **non-nitro** OOM come from the nitrate group ($-ONO_2$):

$$n_{O_{eff}} = n_O - 2 \times n_N \quad (8)$$

S4 Main peaks of 7 discussed non-nitrated-phenols factors

S4.1 Arom-OOM factor

Table S2. Molecular characteristics of the Arom-OOM factor. Presented as several sets of compounds, and the members of each set differ in the addition of a $-CH_2$ moiety. Only the signals that account for more than one thousandth of the factor are selected to reduce uncertainties. The clustering reagent ion NO_3^- or $HNO_3NO_3^-$ has been omitted from the formulas.

No.	Formulas	Contribution to the factor (%)	DBE	n_O	n_N
1	$C_xH_{2x-5}O_6N$, x= [6, 12]	15.0	3	6	1
2	$C_xH_{2x-3}O_6N$, x= [6, 12]	8.8	2	6	1
3	$C_xH_{2x}O_7N_2$, x= [4, 14]	5.5	0	7	2

4	$C_xH_{2x-5}O_7N$, x= [7, 11]	3.9	3	7	1
5	$C_xH_{2x-1}O_5N$, x= [4, 14]	3.9	1	5	1
6	$C_xH_{2x+1}O_5N$, x= [4, 13]	3.4	0	5	1
7	$C_xH_{2x-1}O_6N$, x= [4, 12]	3.1	1	6	1
8	$C_xH_{2x-5}O_8N$, x= [7, 11]	2.5	3	8	1
9	$C_xH_{2x-3}O_7N$, x= [6, 10]	2.2	2	7	1
10	$C_xH_{2x-3}O_5N$, x= [7, 13]	1.9	2	5	1

S4.2 Aliph-OOM-I factor

Table S3. Molecular characteristics of the Aliph-OOM I factor. Presented as several sets of compounds, and the members of each set differ in the addition of a -CH_2 moiety. Only the signals that account for more than one thousandth of the factor are selected to reduce uncertainties. The clustering reagent ion NO_3^- or $HNO_3NO_3^-$ has been omitted from the formulas.

No.	Formulas	Contribution to the factor (%)	DBE	n_O	n_N
1	$C_xH_{2x-3}O_6N$, x= [5, 13]	12.6	2	6	1
2	$C_xH_{2x}O_7N_2$, x= [4, 14]	9.9	0	7	2
3	$C_xH_{2x-1}O_5N$, x= [4, 14]	6.8	1	5	1
4	$C_xH_{2x-2}O_8N_2$, x= [5, 13]	5.0	1	8	2
5	$C_xH_{2x-1}O_6N$, x= [5, 12]	3.8	1	6	1
6	$C_xH_{2x-4}O_4$, x= [6, 11]	2.8	3	4	0
7	$C_xH_{2x-2}O_7N_2$, x= [6, 14]	2.1	1	7	2
8	$C_xH_{2x-5}O_6N$, x= [6, 12]	2.1	3	6	1
9	$C_xH_{2x-2}O_4$, x= [6, 10]	2.1	2	4	0
10	$C_xH_{2x-3}O_7N$, x= [6, 12]	1.7	2	7	1

S4.3 Aliph-OOM-II factor

Table S4. Molecular characteristics of the Aliph-OOM II factor. Presented as several sets of compounds, and the members of each set differ in the addition of a -CH_2 moiety. Only the signals that account for more than one thousandth of the factor are selected to reduce uncertainties. The clustering reagent ion NO_3^- or $HNO_3NO_3^-$ has been omitted from the formulas.

No.	Formulas	Contribution to the factor (%)	DBE	n_O	n_N
1	$C_xH_{2x}O_7N_2$, x= [4, 13]	25.3	0	7	2
2	$C_xH_{2x-1}O_5N$, x= [4, 10]	6.7	1	6	1
3	$C_xH_{2x-2}O_8N_2$, x= [5, 13]	6.2	1	8	2
4	$C_xH_{2x-3}O_6N$, x= [5, 10]	5.0	2	6	1

5	$C_xH_{2x-2}O_7N_2$, x= [5, 13]	4.3	1	7	2
6	$C_xH_{2x-1}O_9N_3$, x= [5, 11]	2.0	0	9	3
7	$C_xH_{2x-4}O_8N_2$, x= [7, 12]	1.9	2	8	2
8	$C_xH_{2x-1}O_{10}N_3$, x= [5, 10]	1.2	0	10	3
9	$C_xH_{2x+1}O_5N$, x= [4, 8]	1.2	0	5	1
10	$C_xH_{2x-1}O_6N$, x= [5, 9]	1.2	1	6	1

S4.4 O_3-related-I factor

Table S5. Molecular characteristics of the O_3-related I factor. Presented as several sets of compounds, and the members of each set differ in the addition of a -CH_2 moiety. Only the signals that account for more than one thousandth of the factor are selected to reduce uncertainties. The clustering reagent ion NO_3^- or $HNO_3NO_3^-$ has been omitted from the formulas.

No.	Formulas	Contribution to the factor (%)	DBE	n_O	n_N
1	$C_xH_{2x-3}O_6N$, x= [4, 12]	12.1	2	6	1
2	$C_xH_{2x-1}O_6N$, x= [4, 11]	7.2	1	6	1
3	$C_xH_{2x-3}O_7N$, x= [4, 11]	6.0	2	7	1
4	$C_xH_{2x-2}O_8N_2$, x= [4, 13]	5.9	1	8	2
5	$C_xH_{2x-5}O_7N$, x= [6, 11]	3.3	3	7	1
6	$C_xH_{2x-5}O_8N$, x= [7, 11]	3.1	3	8	1
7	$C_xH_{2x-5}O_6N$, x= [6, 10]	2.7	3	6	1
8	$C_xH_{2x}O_8N_2$, x= [4, 11]	2.5	0	8	2
9	$C_xH_{2x-2}O_9N_2$, x= [4, 11]	2.0	1	9	2
10	$C_xH_{2x-4}O_8N_2$, x= [6, 13]	1.9	2	8	2

S4.5 O_3-related-II factor

Table S6. Molecular characteristics of the O_3-related II factor. Presented as several sets of compounds, and the members of each set differ in the addition of a -CH_2 moiety. Only the signals that account for more than one thousandth of the factor are selected to reduce uncertainties. The clustering reagent ion NO_3^- or $HNO_3NO_3^-$ has been omitted from the formulas.

No.	Formulas	Contribution to the factor (%)	DBE	n_O	n_N
1	$C_xH_{2x-3}O_6N$, x= [4, 10]	11.3	2	6	1
2	$C_xH_{2x-1}O_6N$, x= [4, 9]	4.9	1	6	1
3	$C_xH_{2x-4}O_4$, x= [6, 10]	4.7	3	4	0
4	$C_xH_{2x-3}O_7N$, x= [4, 10]	4.1	2	7	1
5	$C_xH_{2x-4}O_5$, x= [5, 10]	3.8	3	5	0

6	$C_xH_{2x}O_7N_2$, x= [4, 10]	3.5	0	7	2
7	$C_xH_{2x-5}O_6N$, x= [5, 10]	3.1	3	6	1
8	$C_xH_{2x-5}O_7N$, x= [5, 10]	2.8	3	7	1
9	$C_xH_{2x-6}O_5$, x= [6, 10]	2.8	4	5	0
10	$C_xH_{2x-2}O_4$, x= [6, 9]	2.4	2	4	0

S4.6 MT-mixed-OOM factor

Table S7. Molecular characteristics of the MT-mixed-OOM factor. Presented as several sets of compounds, and the members of each set differ in the addition of a -CH_2 moiety. Only the signals that account for more than one thousandth of the factor are selected to reduce uncertainties. The clustering reagent ion NO_3^- or $HNO_3NO_3^-$ has been omitted from the formulas.

No.	Formulas	Contribution to the factor (%)	DBE	n_O	n_N
1	$C_xH_{2x-3}O_6N$, x= [5, 12]	5.0	2	6	1
2	$C_xH_{2x-1}O_5N$, x= [4, 13]	4.8	1	5	1
3	$C_xH_{2x}O_7N_2$, x= [5, 10]	4.7	0	7	2
4	$C_xH_{2x-5}O_6N$, x= [6, 12]	4.6	3	6	1
5	$C_xH_{2x-4}O_4$, x= [6, 11]	3.5	3	4	0
6	$C_xH_{2x-1}O_6N$, x= [4, 11]	3.4	1	6	1
7	$C_xH_{2x+1}O_5N$, x= [4, 10]	3.2	0	5	1
8	$C_xH_{2x-3}O_5N$, x= [4, 12]	2.9	2	5	1
9	$C_xH_{2x-2}O_4$, x= [6, 9]	2.0	2	4	0
10	$C_xH_{2x-4}O_7N_2$, x= [9, 10]	1.5	2	7	2

S4.7 Mixed-OOM factor

Table S8. Molecular characteristics of the Mixed-OOM factor. Presented as several sets of compounds, and the members of each set differ in the addition of a -CH_2 moiety. Only the signals that account for more than one thousandth of the factor are selected to reduce uncertainties. The clustering reagent ion NO_3^- or $HNO_3NO_3^-$ has been omitted from the formulas.

No.	Formulas	Contribution to the factor (%)	DBE	n_O	n_N
1	$C_xH_{2x-3}O_6N$, x= [4, 11]	11.1	2	6	1
2	$C_xH_{2x-1}O_5N$, x= [4, 12]	8.2	1	5	1
3	$C_xH_{2x-5}O_6N$, x= [6, 11]	3.3	3	6	1
4	$C_xH_{2x-2}O_8N_2$, x= [5, 10]	2.5	1	8	2
5	$C_xH_{2x}O_7N_2$, x= [5, 12]	2.5	0	7	2
6	$C_xH_{2x-1}O_6N$, x= [4, 8]	2.1	1	6	1

7	$C_xH_{2x-2}O_4$, x= [6, 9]	2.1	2	4	0
8	$C_xH_{2x-3}O_5N$, x= [4, 12]	1.8	2	5	1
9	$C_xH_{2x-4}O_4$, x= [6, 10]	1.7	3	4	0
10	$C_xH_{2x-6}O_4$, x= [6, 8]	1.3	4	4	0

S5 The additional information of the Arom-OOM factor

The aromatic oxidation proxy represents the aromatic photo-oxidation and can calculate by Eq. (9):

$$Aromatic\ oxidation\ proxy\ =\ k_{OH} \times Aromatics \times J(O^1D) \quad (9)$$

Where k_{OH} is a reaction constant for the photo-oxidation of aromatics.

Here, we add the OH reactivity of monoterpenes to analysis.

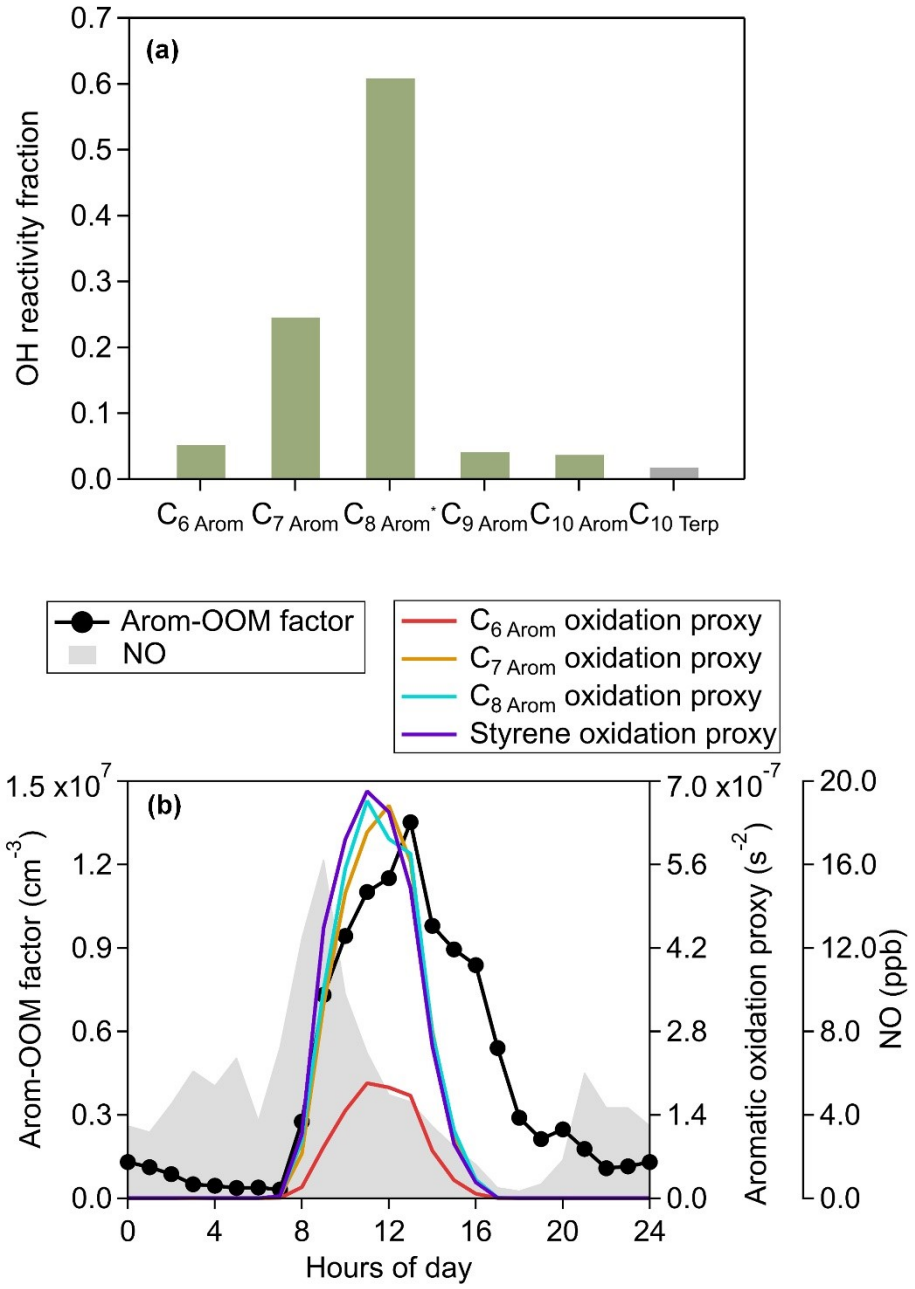

Fig. S8 The analysis of the Arom-OOM factor. (a) The OH reactivity distribution of $C_{6\ Arom}$, $C_{7\ Arom}$, $C_{8\ Arom}$*, $C_{9\ Arom}$, $C_{10\ Arom}$ and $C_{10\ Terp}$ (Note: $C_{8\ Arom}$*= $C_{8\ Arom}$ + Styrene), (b) the median diurnal patterns of Arom-OOM factor and $C_{6\ Arom}$, $C_{7\ Arom}$, $C_{8\ Arom}$, Styrene oxidation proxy.

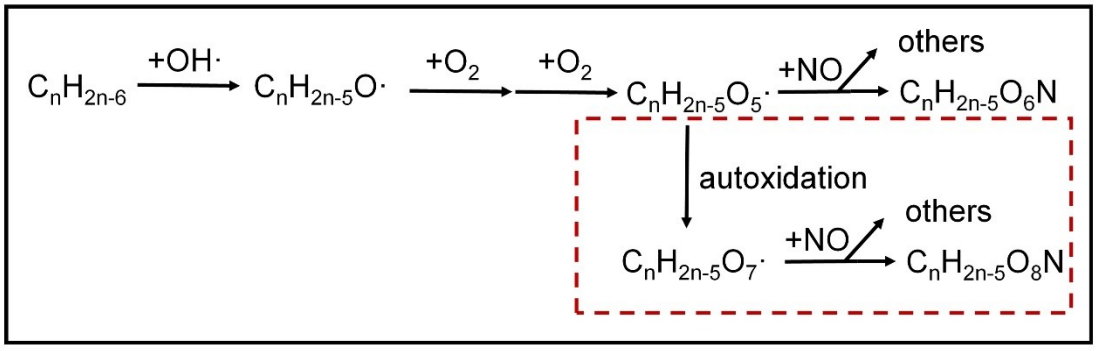

Fig.S9 The potential reaction pathway of the OH-initiated oxidation of aromatics to

form $C_xH_{2x-5}O_6N$ and $C_xH_{2x-5}O_8N$.

S6 The additional information of two Aliph-OOM factors

As described in Liu et al.[6], considering a simple scenario of alkane photo-oxidation under high NO_x conditions: the RO_2 generated from OH attack is completely terminated by NO (Fig. S9(a)). The chain-retaining products are $C_nH_{2n}O$ (one more carbonyl group than the precursor) and $C_nH_{2n+1}O_3N$ (one more nitrate group than the precursor). Further re-oxidation of these products is a repetition of the same process and the 1_{st} - 3_{rd} multi-generation products of alkanes summarized in Fig. S9(b) are regarded as reference compounds, which we compare OOMs with to investigate other mechanisms that differ from those shown in Fig. S9(a). The number of extra oxygen ($^{n_O}{}_{extra}$) from each aliphatic OOM over its corresponding reference molecule was calculated by Eq. (10). The $^{n_O}{}_{extra}$ can represent the extra oxygenated moieties with other processes.

The $^{n_O}{}_{extra}$ is calculated by Eq. (10):

$$n_{O_{extra}} = n_O - DBE - 3 \times n_N \quad (10)$$

Where the DBE is calculated based on Eq. (4).

As showed in Fig. S9(c), two Aliph-OOM factors are mainly dominated by second and third generation products and Aliph-OOM-I factor contains more carbonyl group while Aliph-OOM-II factor prefers to contain nitrate groups.

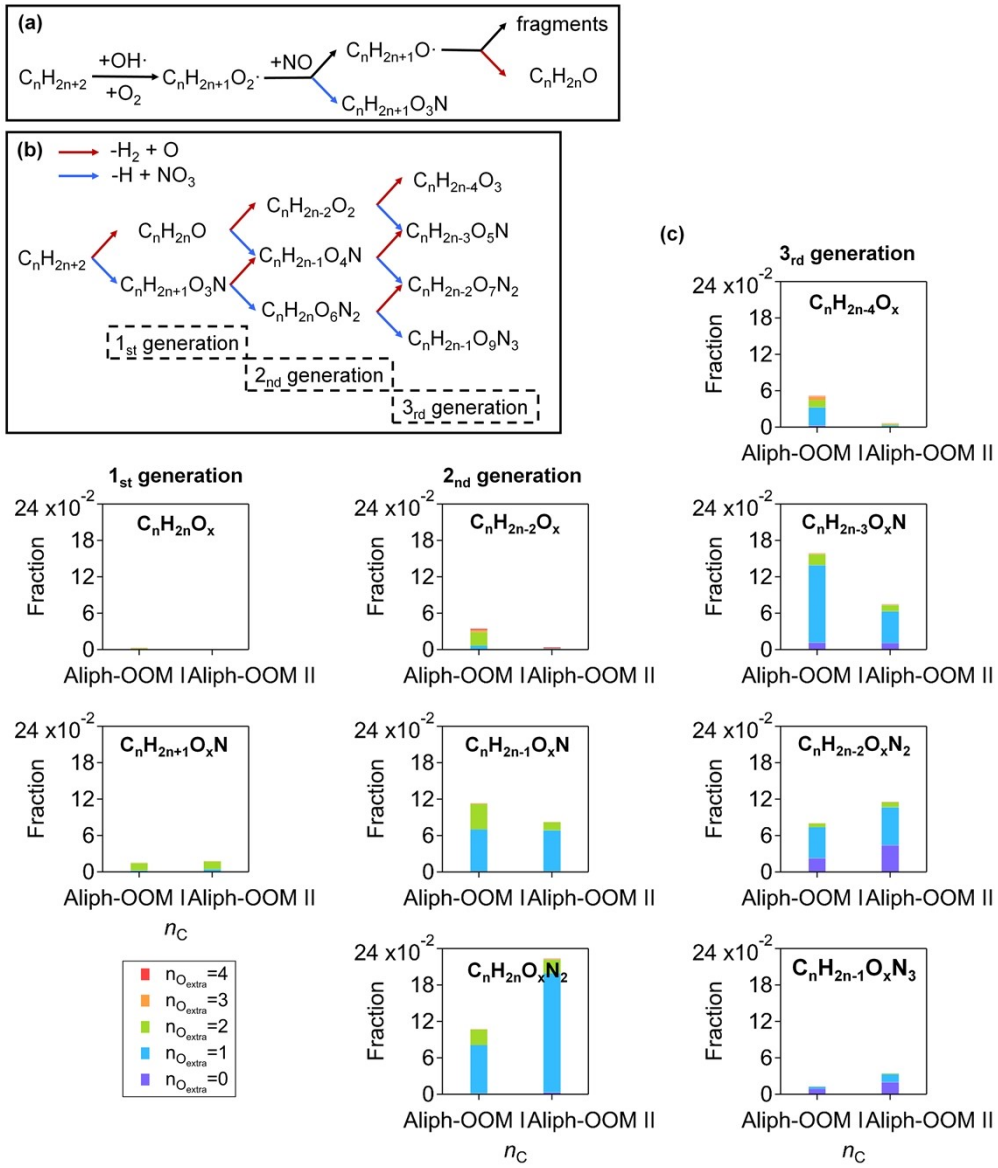

Fig. S10 The multi-generation oxidation of two Aliph-OOM factors. (a) and (b) is adopted from Liu et al.[6]. (c)The compounds with same number of carbon, hydrogen, and nitrogen atoms but different numbers of oxygen atoms are grouped according to the molecular formulas in (b).The bars in (c) are colored with $n_{O_{extra}}$.

S7 The additional information of two O_3-related factors

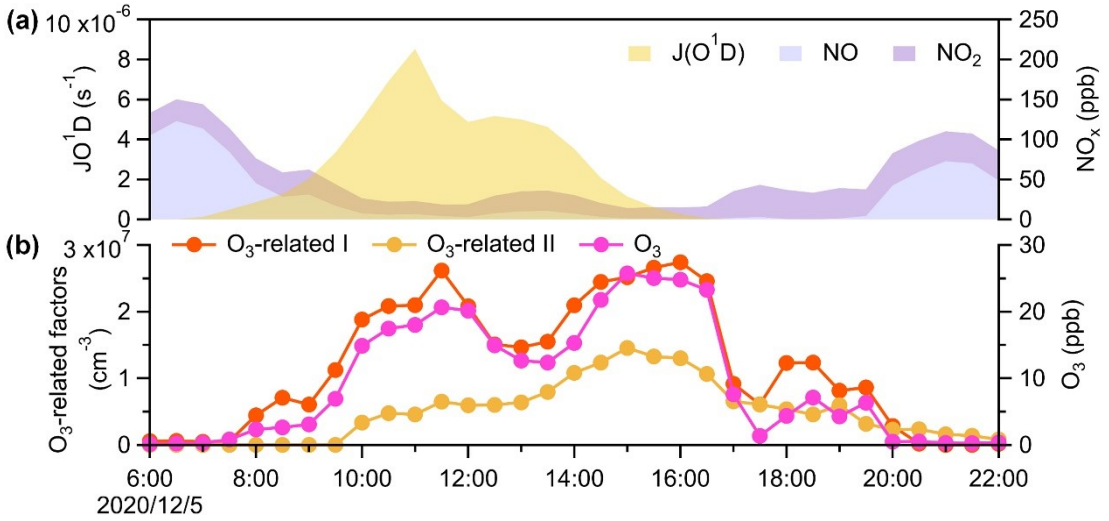

Fig.S11 The time series of select case that O_3-related factors follow O_3 varies, (a) $J(O^1D)$ and NO_x, (b) O_3-related I, O_3-related II and O_3.

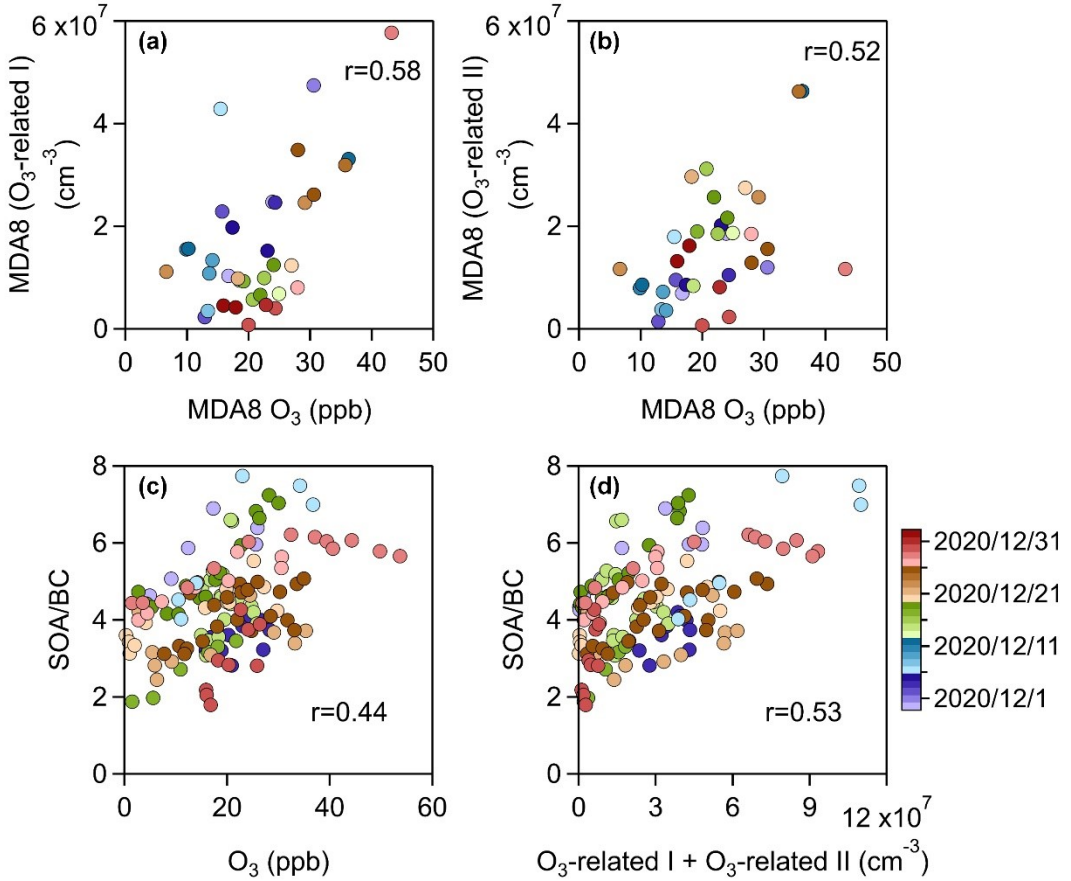

Fig.S12 Scatter plots of (a) the maximum daily 8-h average (MDA8) O_3-related I , and (b) MDA8 O_3-related II with MDA8 O_3, secendary organic aerosol(SOA) to black carbon(BC) ratio with (c) ozone and (d) two O_3-related factors in 17 ozone production cases.

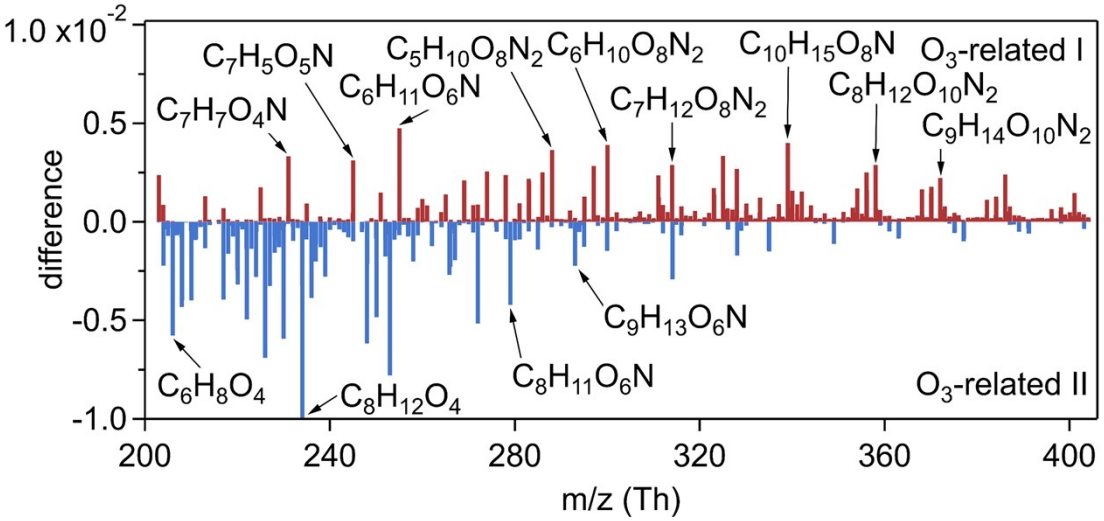

Fig. S13 The difference in mass-to-charge of the O_3-related-I factor and O_3-related-II factor.

S8 The additional information of the Mixed-OOM and the MT-mixed-OOM factors

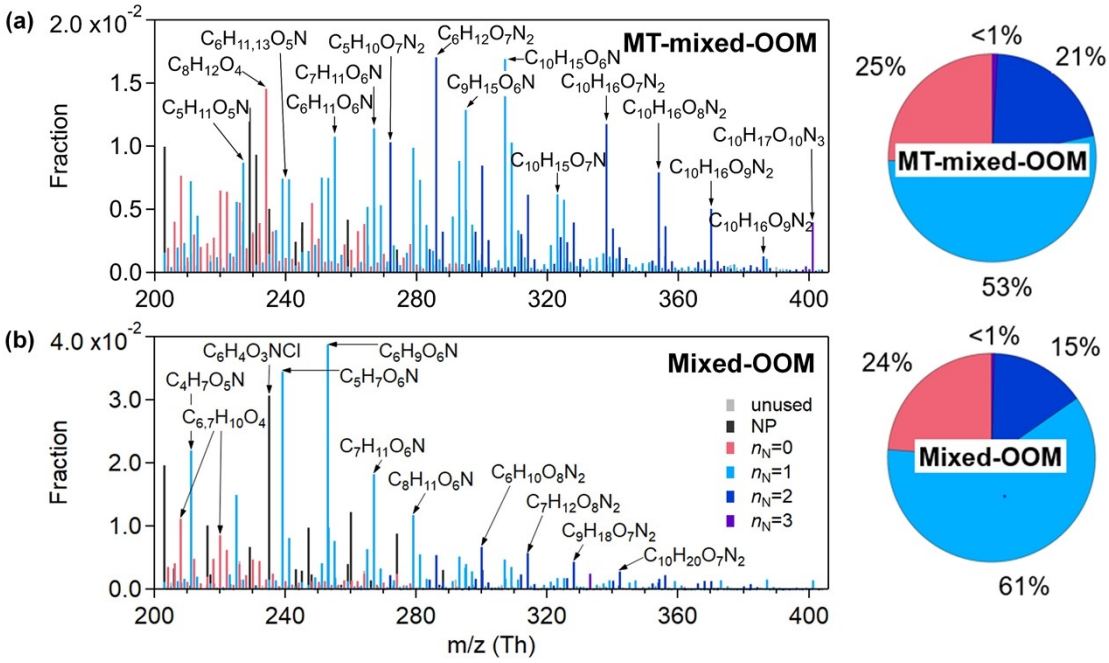

Fig. S14 Profiles of 2 binPMF factors. Mass spectra and pie of (a) the MT-mixed-OOM factor, (b) the Mixed-OOM factor. The elemental formulas of major peaks are labeled above them. Peaks are color-coded by n_N, and the fractions of peaks grouped by n_N are reported in the pie chart for each factor. The gray sticks are fluorinated contaminations, or non-identified compounds. The nitrated phenols are drawn separately with black peaks. So n_N can more reliably represent the number of nitrate groups in each molecule.

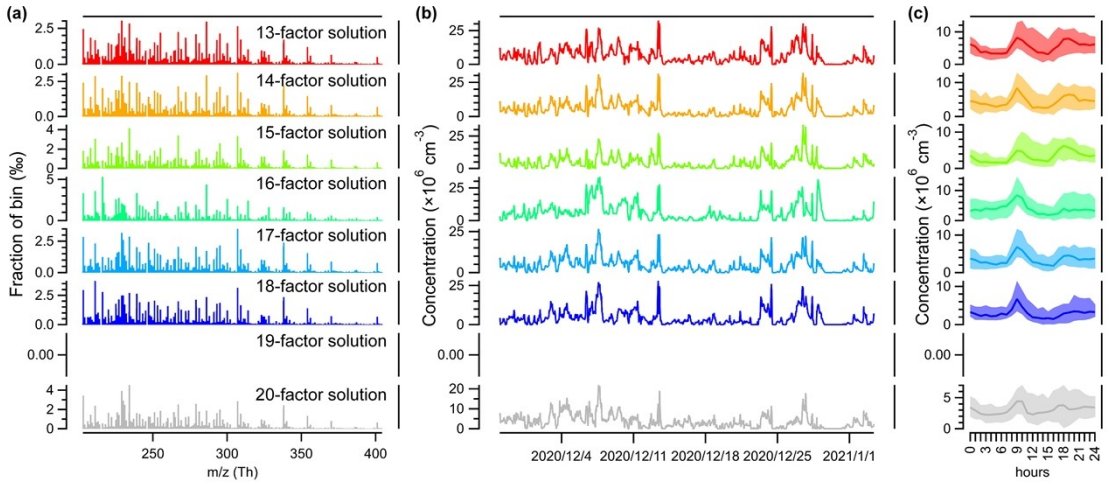

Fig. S15 Evolution of the MT-mixed-OOM factor. (a) profiles, (b) time series, and (c) diurnal patterns.

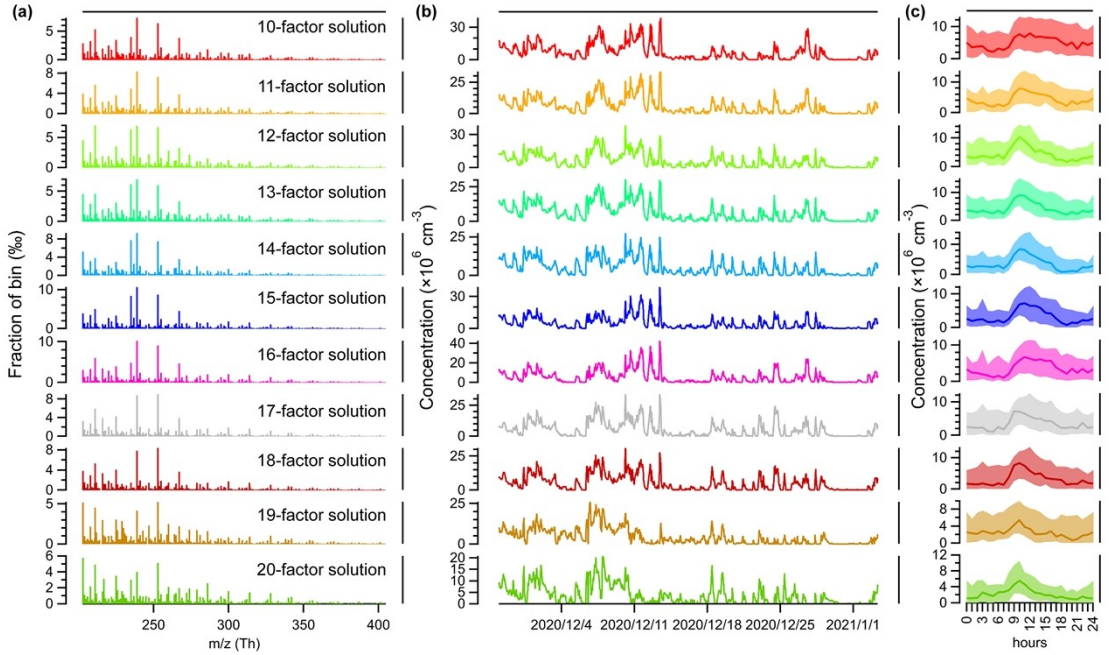

Fig. S16 Evolution of the Mixed-OOM factor. (a) profiles, (b) time series, and (c) diurnal patterns.

S9 The additional information of NP factors

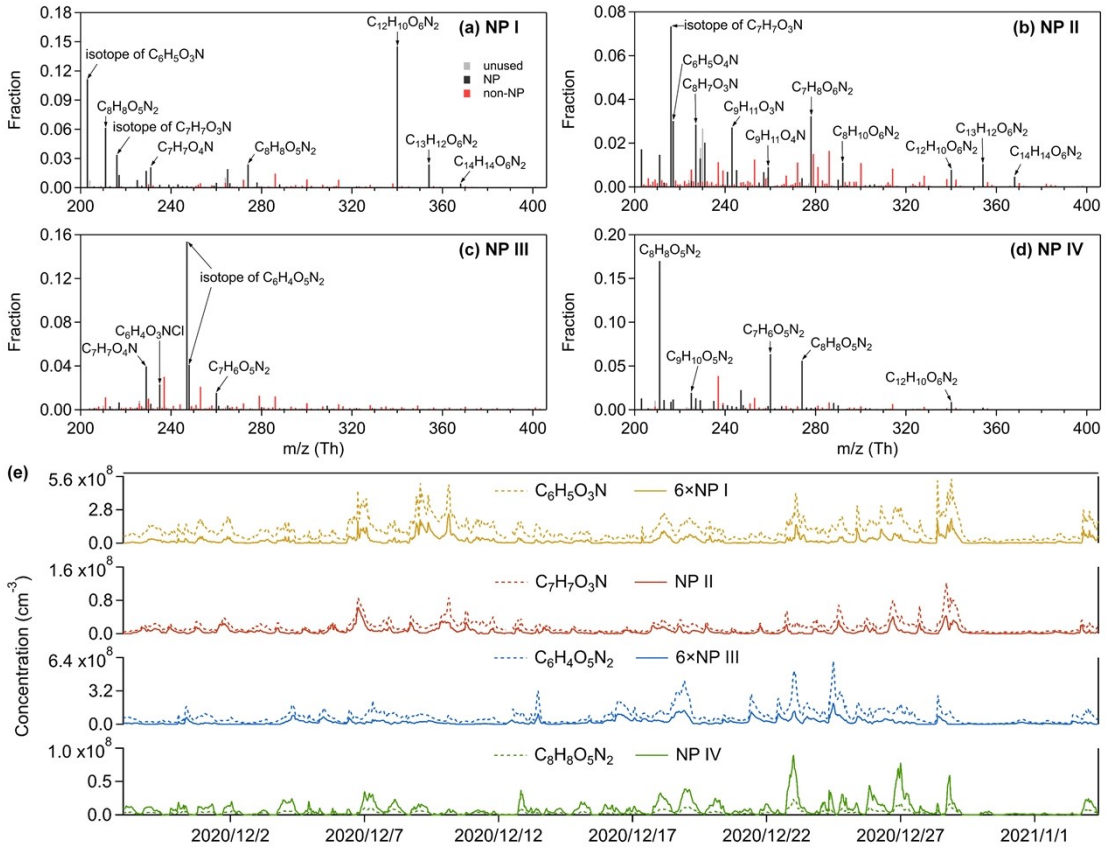

Fig. S17 Profiles of NP factors. Mass spectra and pie of (a) NP-I factor, (b) NP-II factor, (c) NP-III, (d) NP-IV.The time series of four factors and their traces was ploted in (e). The nitrated phenols are drawn separately with black peaks in (a–d), while other OOMs are plotted as red peaks.

S10 The molecular information of the high-quality OOMs dataset

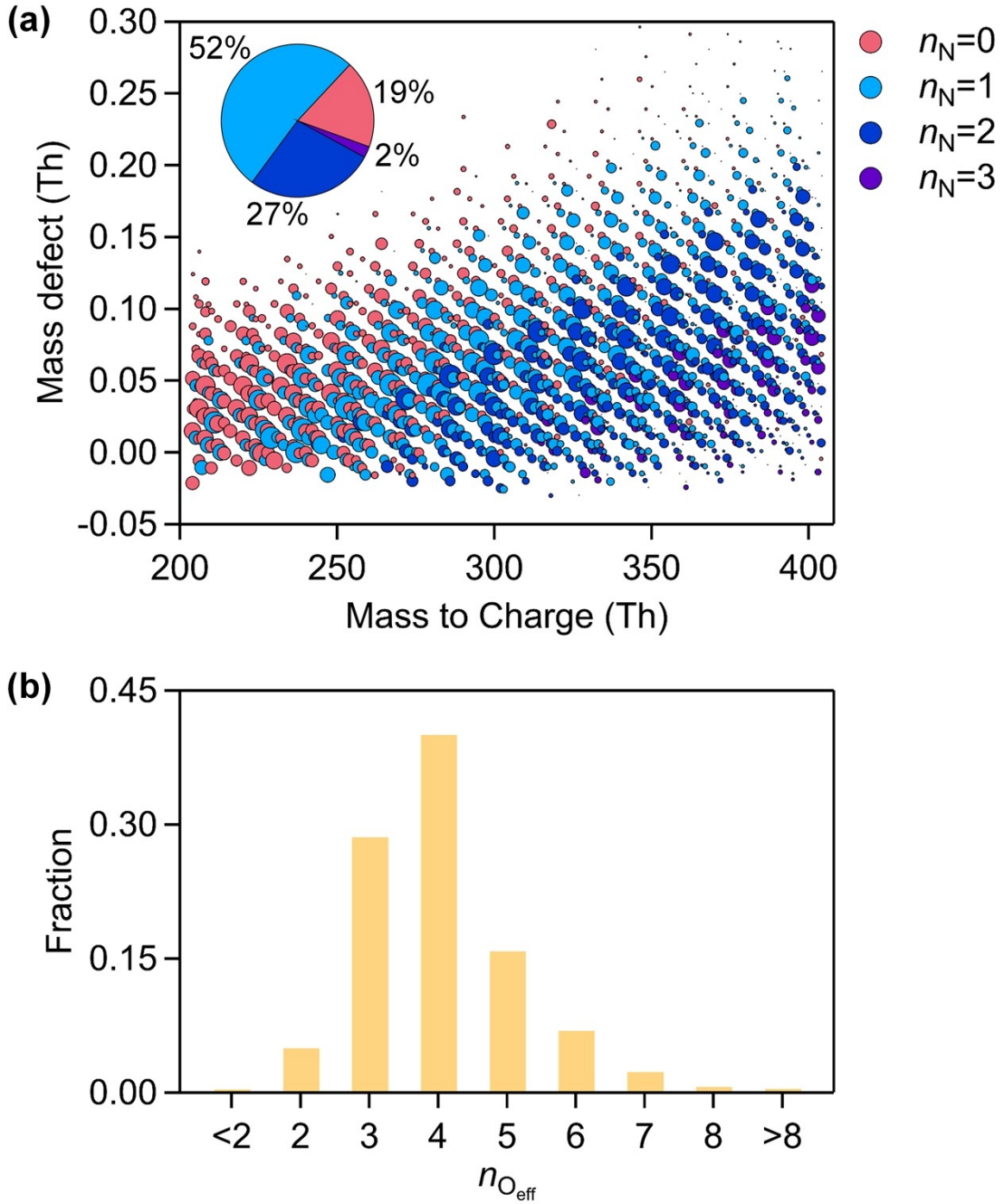

Fig. S18 The molecular information of the high-quality OOMs dataset. (a) Mass defect plot of the OOMs dataset. The x axis shows the exact mass of the OOMs and y axis shows their mass defect (exact mass subtracted by its unit mass). The color of the marker point represents n_N and the size of the marker point corresponds to the concentration of OOMs, (b) the distribution of OOMs dataset grouped by $n_{O_{eff}}$.

S11 Relationship of OOMs with O_3, $PM_{2.5}$

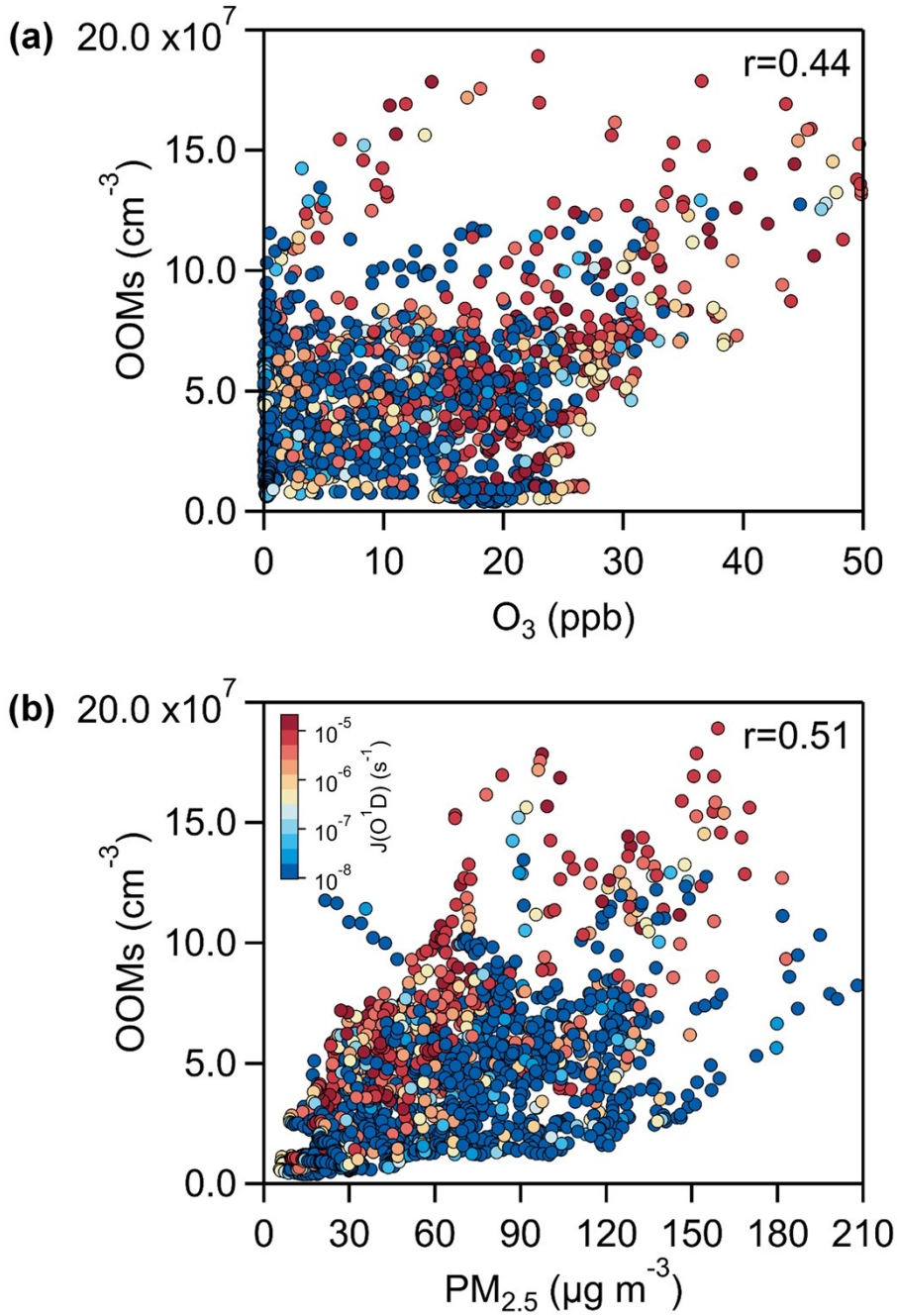

Fig. S19 The scatter plot of OOMs with (a) O_3, (b) $PM_{2.5}$ in all time, each dot is colored by $J(O^1D)$.

S12 Relationship of $PM_{2.5}$ with O_x and PAN

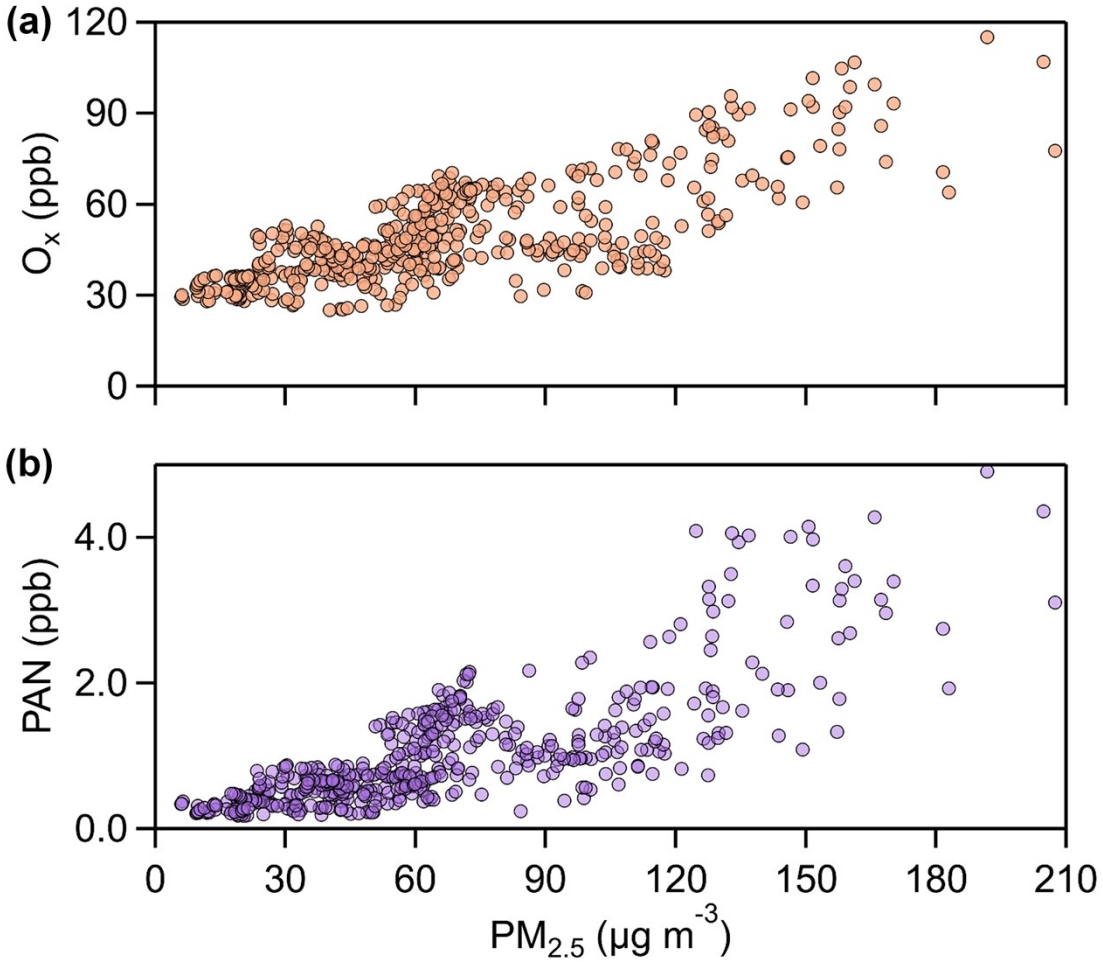

Fig. S20 The scatter plot of $PM_{2.5}$ with (a) O_x ($O_x = O_3 + NO_2 + NO_z$, $NO_z = NO_y - NO_x$), (b) PAN in the daytime.

S13 The calculation of OH proxy

The OH proxy is calculated by applying the Eq. (11):

$$OH\ proxy = \frac{[H_2SO_4] \times CS}{[SO_2]} \tag{11}$$

Where the value of CS was calculated following Eq. (14)[11]:

$$CS = 2\pi D \sum_i \beta_{m_i} d_{p_i} N_i \tag{12}$$

Where D is the diffusion coefficient of gaseous sulfuric acid, βm is a transition-regime correction factor dependent on the Knudsen number[12], and d_{p_i} and N_i are the diameter and number concentration of particles in size bin i.

Reference

1. Y. J. Zhang, O. Perakyla, C. Yan, L. Heikkinen, M. Aijala, K. R. Daellenbach, Q. Z. Zha, M. Riva, O. Garmash, H. Junninen, P. Paatero, D. Worsnop and M. Ehn, A novel approach for simple statistical analysis of high-resolution mass spectra, *Atmospheric Measurement Techniques*, 2019, **12**, 3761-3776.
2. A. V. Polissar, P. K. Hopke, P. Paatero, W. C. Malm and J. F. Sisler, Atmospheric aerosol over Alaska: 2. Elemental composition and sources, *Journal of Geophysical Research: Atmospheres*, 1998, **103**, 19045-19057.
3. J. D. Allan, J. L. Jimenez, P. I. Williams, M. R. Alfarra, K. N. Bower, J. T. Jayne, H. Coe and D. R. Worsnop, Quantitative sampling using an Aerodyne aerosol mass spectrometer 1. Techniques of data interpretation and error analysis, *Journal of Geophysical Research: Atmospheres*, 2003, **108**, 4283.
4. C. Yan, W. Nie, M. Äijälä, M. P. Rissanen, M. R. Canagaratna, P. Massoli, H. Junninen, T. Jokinen, N. Sarnela, S. A. K. Häme, S. Schobesberger, F. Canonaco, L. Yao, A. S. H. Prévôt, T. Petäjä, M. Kulmala, M. Sipilä, D. R. Worsnop and M. Ehn, Source characterization of highly oxidized multifunctional compounds in a boreal forest environment using positive matrix factorization, *Atmospheric Chemistry and Physics*, 2016, **16**, 12715-12731.
5. Q. Zhang, J. L. Jimenez, M. R. Canagaratna, I. M. Ulbrich, N. L. Ng, D. R. Worsnop and Y. Sun, Understanding atmospheric organic aerosols via factor analysis of aerosol mass spectrometry: a review, *Anal Bioanal Chem*, 2011, **401**, 3045-3067.
6. Y. Liu, W. Nie, Y. Li, D. Ge, C. Liu, Z. Xu, L. Chen, T. Wang, L. Wang, P. Sun, X. Qi, J. Wang, Z. Xu, J. Yuan, C. Yan, Y. Zhang, D. Huang, Z. Wang, N. M. Donahue, D. Worsnop, X. Chi, M. Ehn and A. Ding, Formation of condensable organic vapors from anthropogenic and biogenic volatile organic compounds (VOCs) is strongly perturbed by NOx in eastern China, *ATMOSPHERIC CHEMISTRY AND PHYSICS*, 2021, **21**, 14789-14814.
7. J. H. Kroll, N. M. Donahue, J. L. Jimenez, S. H. Kessler, M. R. Canagaratna, K. R. Wilson, K. E. Altieri, L. R. Mazzoleni, A. S. Wozniak, H. Bluhm, E. R. Mysak, J. D. Smith, C. E. Kolb and D. R. Worsnop, Carbon oxidation state as a metric for describing the chemistry of atmospheric organic aerosol, *Nature Chemistry*, 2011, **3**, 133-139.
8. N. M. Donahue, S. A. Epstein, S. N. Pandis and A. L. Robinson, A two-dimensional volatility basis set: 1. organic-aerosol mixing thermodynamics, *Atmospheric Chemistry and Physics*, 2011, **11**, 3303-3318.
9. D. Stolzenburg, L. Fischer, A. L. Vogel, M. Heinritzi, M. Schervish, M. Simon, A. C. Wagner, L. Dada, L. R. Ahonen, A. Amorim, A. Baccarini, P. S. Bauer, B. Baumgartner, A. Bergen, F. Bianchi, M. Breitenlechner, S. Brilke, S. B. Mazon, D. Chen, A. Dias, D. C. Draper, J. Duplissy, I. El Haddad, H. Finkenzeller, C. Frege, C. Fuchs, O. Garmash, H. Gordon, X. He, J. Helm, V. Hofbauer, C. R. Hoyle, C. Kim, J. Kirkby, J. Kontkanen, A. Kuerten, J. Lampilahti, M. Lawler, K. Lehtipalo, M. Leiminger, H. Mai, S. Mathot, B. Mentler, U. Molteni, W. Nie, T. Nieminen, J. B. Nowak, A. Ojdanic, A. Onnela, M. Passananti, T. Petaja, L. L. J. Quelever, M. P. Rissanen, N. Sarnela, S. Schallhart, C. Tauber, A. Tome, R. Wagner, M. Wang, L. Weitz, D. Wimmer, M. Xiao, C. Yan, P. Ye, Q. Zha, U. Baltensperger, J. Curtius, J. Dommen, R. C. Flagan, M.

Kulmala, J. N. Smith, D. R. Worsnop, A. Hansel, N. M. Donahue and P. M. Winkler, Rapid growth of organic aerosol nanoparticles over a wide tropospheric temperature range, *Proc. Natl. Acad. Sci. U. S. A.*, 2018, **115**, 9122-9127.

10. S. A. Epstein, I. Riipinen and N. M. Donahue, A Semiempirical Correlation between Enthalpy of Vaporization and Saturation Concentration for Organic Aerosol, *Environmental Science & Technology*, 2010, **44**, 743-748.

11. M. Kulmala, T. Petaja, T. Nieminen, M. Sipila, H. E. Manninen, K. Lehtipalo, M. Dal Maso, P. P. Aalto, H. Junninen, P. Paasonen, I. Riipinen, K. E. Lehtinen, A. Laaksonen and V. M. Kerminen, Measurement of the nucleation of atmospheric aerosol particles, *Nat Protoc*, 2012, **7**, 1651-1667.

12. N. A. Fuchs and A. G. Sutugin, in *Topics in Current Aerosol Research*, eds. G. M. Hidy and J. R. Brock, Pergamon, 1971, p. 1.